J. Am. Soc. Mass Spectrom. (2018) 29:2110–2113
DOI: 10.1007/s13361-018-2040-9

APPLICATION NOTE

Resolution-Enhanced Kendrick Mass Defect Analysis of Polycyclic Aromatic Hydrocarbons and Fullerenes in the Diffusion Flame from a Butane Torch

Robert B. Cody,[1] Thierry Fouquet[2]

[1]JEOL USA, Inc., 11 Dearborn Rd., Peabody, MA 01960, USA
[2]Research Institute for Sustainable Chemistry, National Institute for Advanced Industrial Science and Technology (AIST), Tsukuba, 305-8565, Japan

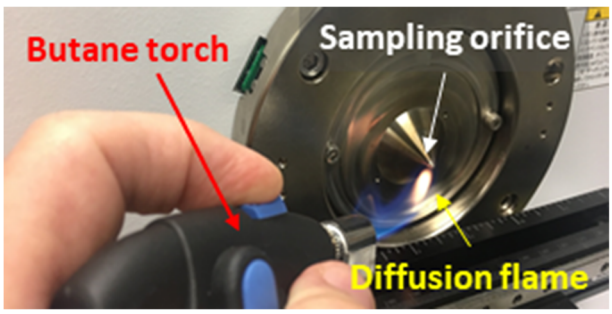

Abstract. A modified Kendrick Mass Defect (KMD) analysis was applied to the analysis of polycyclic aromatic hydrocarbons (PAHs) and fullerenes in the diffusion flame from a handheld butane torch.

Keywords: Data analysis, Kendrick, Flame, Fullerene, Carbon clusters, PAH, Mass defect

Received: 31 May 2018/Revised: 18 July 2018/Accepted: 19 July 2018/Published Online: 6 August 2018

Introduction

Kendrick mass defect analysis [1] is widely used for the interpretation of high-resolution mass spectra of petrochemicals. The Kendrick mass KM is related to the IUPAC mass by

$$\mathrm{KM} = \text{observed IUPAC mass} \times \text{nominal mass of } CH_2 / \text{exact mass of } CH_2 \quad (1)$$

The Nominal Kendrick Mass (NKM) is the nearest integer Kendrick mass, and the Kendrick mass defect KMD is defined as

$$\mathrm{KMD} = \mathrm{NKM} - \mathrm{KM} \quad (2)$$

Kendrick mass defect analysis can be applied to any compounds that differ by a repeating composition ("base unit") such as polymers [2–6], bacterial fatty acids [4], or halogen-substituted compounds of environmental interest [7]. The Kendrick mass KM expression in Eq. (1) can be generalized to

$$\mathrm{KM} = \text{observed IUPAC mass} \times \text{nominal mass of repeat unit} / \text{IUPAC mass of repeat unit} \quad (3)$$

Recently, Fouquet and Sato showed that using fractional base units can dramatically improve the resolution of Kendrick mass defect analysis [8]. Fractional base units modify the *variation* of mass defects when changing the elemental composition. Using a C/11 base unit, replacing ^{12}C by ^{13}C leads to a variation of mass defect increased by a factor of 24 compared to a C base unit. Consequently, using C/X instead of C spreads points along the whole defect range taking full advantage of the spectral width of the plot. Here, we extend Kendrick mass defect analysis with fractional base units to carbon clusters and polycyclic aromatic hydrocarbons (PAHs) using the IUPAC mass (C = 12.00000) as the base unit.

There are many reports on the formation of PAHs and carbon clusters, including fullerenes, in flames [9–21]. The mechanism of fullerene production has been discussed in the literature, and it has been proposed that PAHs are the

Correspondence to: Robert Cody; *e-mail:* cody@jeol.com

precursors of fullerenes [16, 17]. For background on the mechanisms of ion formation in flames the reader is directed to Calcote's classic paper [22] and an extensive review by Fialkov [23]. Here, we do not address the mechanism of carbon cluster ion formation in flames, but focus on data visualization tools for high-resolution mass spectra of the cluster ions and PAHs.

Experimental

The diffusion flame from a handheld butane torch (ST2200T-Detail Torch, BernzOmatic, Rochester, NY) was introduced directly into the sampling orifice ("Orifice 1") of a commercial reflectron time-of-flight mass spectrometer (AccuTOF™-DART® 4G, JEOL USA, Inc.). The direct analysis in real time (DART-SVP, IonSense LLC, Saugus MA USA) ion source was retracted to permit access to the sampling orifice of the mass spectrometer atmospheric pressure interface. The DART mounting flange provided a magnetic safety interlock to allow the collection of mass spectra from the flame. Ions were sampled directly into the sampling orifice (designated "Orifice 1") from the diffusion flame. The mass spectral acquisition rate was 1 spectrum s^{-1} and the resolving power was > 10,000 (FWHM). Positive-ion atmospheric pressure interface potentials were orifice 1 = +20 V, ring lens = +5 V, and orifice 2 = +5 V. The RF ion guide potential was raised from 600 to 2000 V after no significant peaks were observed in the diffusion flame spectra below *m/z* 200. Although abundant peaks in the low-mass region were observed in other regions of the premixed flame, this was not the case for the diffusion flame where abundant fullerenes were observed. Polarities were reversed for acquisition of negative-ion mass spectra. Jeffamine M-600 and Fomblin Y were measured using the DART ion source as external mass calibration standards [24, 25].

Fluctuations could be observed in the mass spectrum depending on the exact location in the flame that was being sampled. Abundant fullerenes were observed for the soot-forming region near the tip of the diffusion flame. Mass spectra with relatively abundant carbon clusters and fullerenes were selected for the examples shown herein. Mass Mountaineer software (massmountaineer.com) allowed us to rotate mass defect plots and use the mouse cursor to select regions for further analysis by resolution-enhanced KMD analysis and elemental composition determinations.

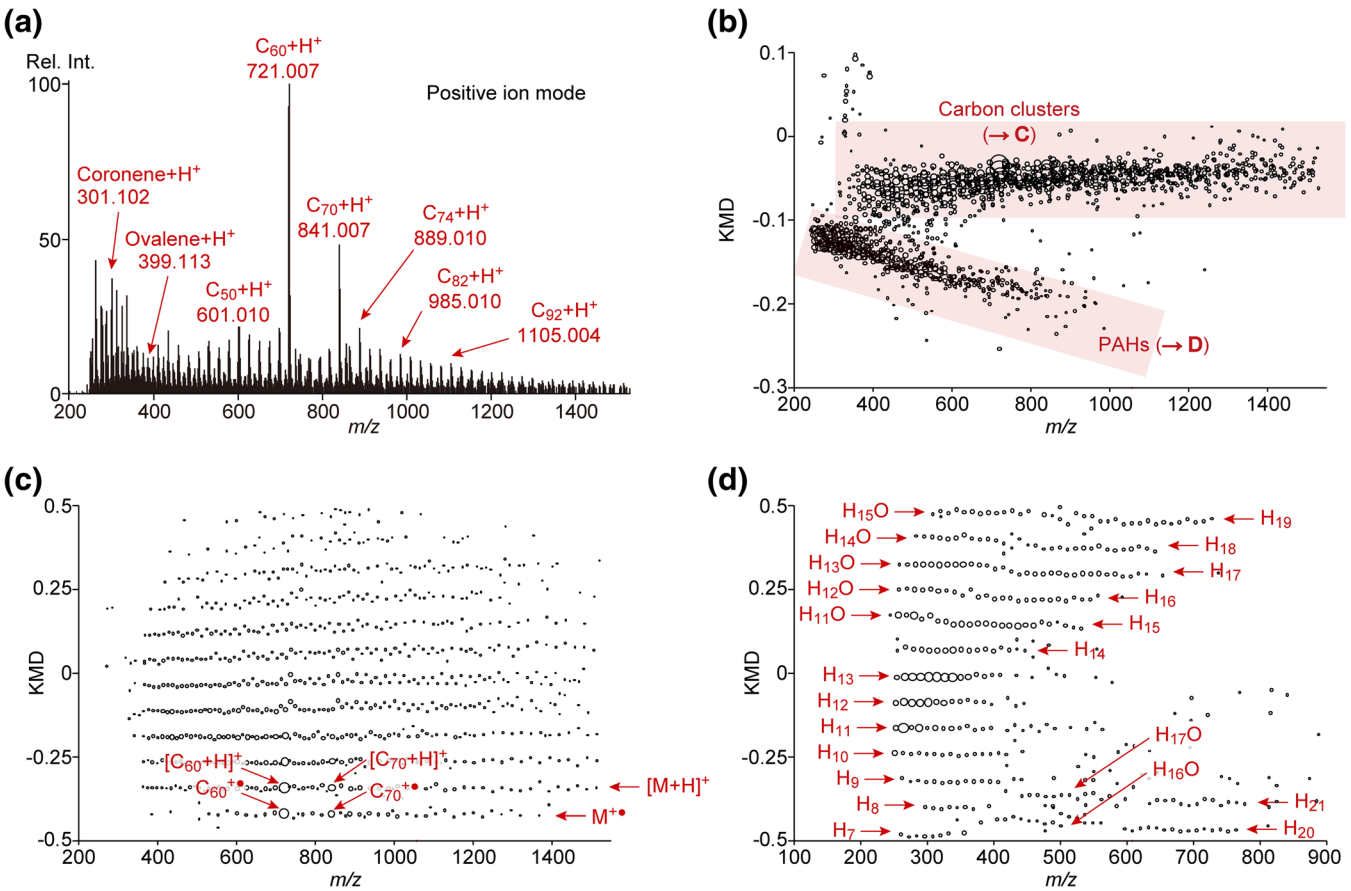

Figure 1. (**a**) Positive-ion mass spectrum of the butane diffusion flame, (**b**) mass defect plot showing separate clusters for PAHs and carbon clusters, (**c**) resolution-enhanced Kendrick mass defect plot using C/11 as the base unit for carbon clusters, and (**d**) resolution-enhanced Kendrick mass defect plot using C/11 as the base unit for PAHs. Carbons Cn¬ are omitted from the compositions labeled in (**d**) for readability

Results and Discussion

Although a previous study reported that fullerenes were not observed in soot from butane diffusion flames in the absence of chlorinated hydrocarbons [14], the positive-ion mass spectrum of the ions we observed in the diffusion flame was dominated by molecular ions and protonated molecules for PAHs, carbon clusters, and fullerenes (Figure 1a). A simple mass defect plot (mass defect vs. *m/z*) shows two separate clusters for the PAHs and the carbon clusters (Figure 1b). Mass Mountaineer software was used to highlight and isolate each of the two clusters for further analysis with resolution-enhanced Kendrick mass defect analysis.

The resolution-enhanced KMD plot of the carbon clusters using a fractional base unit corresponding to C/11 (Figure 1c) shows separation of the molecular ions $M^{+\bullet}$ and the protonated molecules $[M+H]^+$ and isotopic peaks. The C/11 base unit is effective in separating $C_{60}^{+\bullet}$ and $C_{60}H^+$ and isotopic peaks for both species. The mass spectrum for each of these species can be examined by highlighting each region in the resolution-enhanced KMD plot. The resolving power of the reflectron TOF mass analyzer is insufficient to separate $^{12}C_{59}{}^{13}C_1{}^+$ and $^{12}C_{60}H^+$.

The resolution-enhanced KMD plot for the PAH cluster is shown in Figure 1d. By using a C/11 base unit, positive ions with the general composition C_nH_x appear along horizontal lines. Each horizontally aligned group has a constant number *x* of hydrogens ($7 \le x \le 22$) and varying numbers *n* of carbons ($20 \le n \le 60$). The points fall within the compositional space boundaries proposed by Lobodin et al. [26] in that the double bond equivalents do not exceed 90% of the number of carbons. Additional species can be identified in the resolution-enhanced KMD plot at lower *m/z* that do not fall along the lines for C_nH_x species. These are identified by exact mass measurements as oxidized species having the composition $C_{18\text{-}41}H_{11\text{-}15}O^+$.

The mass spectrum of the negative ions in the diffusion flame is shown in Figure 2a. Abundant ions are observed in the range above approximately *m/z* 400, extending beyond *m/z* 2000. While the peak for $C_{60}^{-\bullet}$ is clearly more abundant than neighboring peaks, the most abundant peak in the mass spectrum is $[C_{82}+H]^-$. The mass defect plot in Figure 2b shows points that essentially fall along a straight line.

This plot does not provide any useful information about the species present in the negative-ion mass spectrum except for the fact that there are compositions present that differ only by the number of carbons. In contrast, the resolution-enhanced

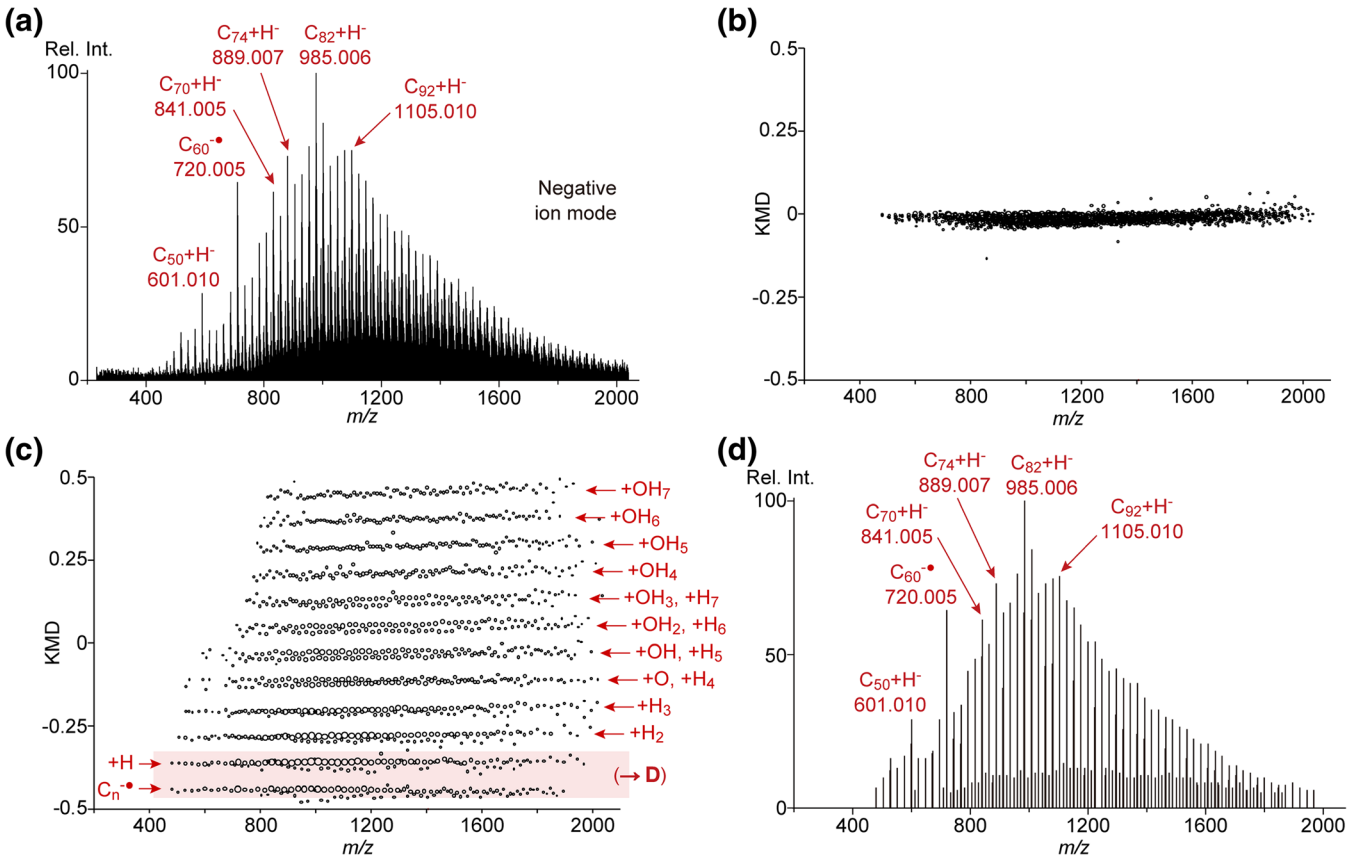

Figure 2. (**a**) Negative-ion mass spectrum of the butane diffusion flame, (**b**) conventional mass defect plot for the mass spectrum in (**a**), (**c**) resolution-enhanced KMD plot using C/11 as the base unit for the negative ions, and (**d**) molecular ion peaks and hydride-attachment peaks extracted from (**a**) for the C/11 Kendrick mass defect range –0.04 to +0.11. Carbons C_n are omitted from the compositions labeled in (**c**) for readability

KMD plot using C/11 as the base unit (Figure 2c) shows a number of distinct species. The most abundant species are molecular ions $C_n^{-\bullet}$ and ions attributed to hydride attachment $[C_n + H]^-$. All of the peaks are assigned the general composition $C_nH_xO_y^-$ where $0 \le x \le 6$ and y is 0 or 1. For all carbon clusters except C_{60}, hydride attachment peaks are more abundant than the molecular ion peaks. The resolution-enhanced KMD plot can be used to select and isolate series of compounds that have the same fractional-base-unit mass defect for examination or further analysis. For example, Figure 2d shows a mass spectrum molecular ion peaks and hydride-attachment peaks separated from the less-abundant peak series. This was accomplished by selecting the components having C/11 mass defects within the range −0.04 to +0.11.

Conclusion

Resolution-enhanced KMD plots were created for carbon clusters and PAHs by using fractional IUPAC base units (C/n). The enhanced KMD plot using C/11 base units for the PAHs provided a simple way to visualize PAHs with differing numbers of hydrogens and revealed the presence of oxidized species with the compositions $C_{18\text{-}41}H_{11\text{-}15}O^+$. The negative-ion mass spectrum of the diffusion flame showed peaks extending from *m/z* 400 to beyond *m*/z 2000. The Kendrick enhanced mass defect using C/11 base units for the negative-ion mass spectrum revealed abundant molecular ions ($C_n^{-\bullet}$), hydride attachment $[C_n + H]^-$ peaks, and minor peaks with compositions $C_{39\text{-}168}H_{0\text{-}7}O_{0\text{–}1}^-$. Interestingly, the most abundant peak was not $C_{60}^{-\bullet}$, but $[C_{82} + H]^-$.

Funding Information

T. Fouquet gratefully acknowledges the ongoing financial support by the Japan Society for the Promotion of Science (JSPS) under the Postdoctoral Fellowship for Overseas Researchers program (FY2015) and a Grant-in-Aid “JSPS KAKENHI” (Grant number: JP 15F15344).

References

1. Kendrick, E.: A mass scale based on CH2 = 14.0000 for high resolution mass spectrometry of organic compounds. Anal. Chem. **35**, 2146–2154 (1963)
2. Sato, H., Nakamura, S., Teramoto, K., Sato, T.: Structural characterization of polymers by MALDI spiral-TOF mass spectrometry combined with Kendrick mass defect analysis. J. Am. Soc. Mass Spectrom. **25**, 1346–1355 (2014)
3. Fouquet, T., Nakamura, S., Sato, H.: MALDI SpiralTOF high-resolution mass spectrometry and Kendrick mass defect analysis applied to the characterization of poly(ethylene-co-vinyl acetate) copolymers. Rapid Commun. Mass Spectrom. **30**, 973–981 (2016)
4. Teramoto, K., Asamizu, S., Ozaki, T., Satoh, K., Onaka, H., Cody, R.B.: MALDI spiral-TOFMS and Kendrick mass defect analysis of mycolic acids from bacteria which accelerate the formation of antibiotics. 64th Conference on Mass Spectrometry and Allied Topics (2016)
5. Fouquet, T., Cody, R.B., Sato, H.: Capabilities of the remainders of nominal Kendrick masses and the referenced Kendrick mass defects for copolymer ions. J. Mass Spectrom. **52**, 618–624 (2017)
6. Cody, R.B., Fouquet, T.: Paper spray and Kendrick mass defect analysis of block and random ethylene oxide/propylene oxide copolymers. Anal. Chim. Acta. **989**, 38–44 (2017)
7. Ubukata, M., Jobst, K.J., Reiner, E.J., Reichenbach, S.E., Tao, Q., Hang, J., Wu, Z., Dane, A.J., Cody, R.B.: Non-targeted analysis of electronics waste by comprehensive two-dimensional gas chromatography combined with high-resolution mass spectrometry: using accurate mass information and mass defect analysis to explore the data. J. Chromatogr. A. **1395**, 152–159 (2015)
8. Fouquet, T., Sato, H.: Extension of the Kendrick mass defect analysis of homopolymers to low resolution and high mass range mass spectra using fractional base units. Anal. Chem. **89**, 2682–2686 (2017)
9. Malhotra, R., Ross, D.S.: Characterization of carbonaceous soots by field ionization mass spectrometry: in search of C60 and other fullerenes. J. Phys. Chem. **95**, 4599–4601 (1991)
10. Howard, J.B.: Fullerenes formation in flames. Symp. Combust. **24**, 933–946 (1992)
11. Pope, C.J., Marr, J.A., Howard, J.B.: Chemistry of fullerenes C60 and C70 formation in flames. J. Phys. Chem. **97**, 11001–11013 (1993)
12. Richter, H., Labrocca, A.J., Grieco, W.J., Taghizadeh, K., Lafleur, A.L., Howard, J.B.: Generation of higher fullerenes in flames. J. Phys. Chem. B. **101**, 1556–1560 (1997)
13. Mansurov, Z.A.: Soot and nanomaterials formation in flame. Eurasian Chemico-Technological Journal. **16**, 169–177 (2014)
14. Fialkov, A.B., Dennebaum, J., Homann, K.H.: The effect of chlorinated hydrocarbons on the formation of positively charged polycyclic aromatic hydrocarbons and fullerenes with masses up to 1300 U in benzene and butane flames. Proc. Combust. Inst. **28**, 2635–2641 (2000)
15. Richter, H., Grieco, W.J., Howard, J.B.: Formation mechanism of polycyclic aromatic hydrocarbons and fullerenes in premixed benzene flames. Combustion and Flame. **119**, 1–22 (1999)
16. Baum, T., Löffler, S., Löffler, P., Weilmünster, P., Homann, K.H.: Fullerene ions and their relation to PAH and soot in low-pressure hydrocarbon flames. Ber. Bunsenges. Phys. Chem. **96**, 841–857 (1992)
17. Reilly, P.T.A., Gieray, R.A., Whitten, W.B., Ramsey, J.M.: Fullerene evolution in flame-generated soot. J. Am. Chem. Soc. **122**, 11596–11601 (2000)
18. Bachmann, M., Wiese, W., Homann, K.H.: PAH and aromers: precursors of fullerenes and soot. Symp. Combust. **26**, 2259–2267 (1996)
19. Homann, K.-H.: Fullerenes and soot formation—new pathways to large particles in flames. Angew. Chem. Int. Ed. **37**, 2434–2451 (1998)
20. Bachmann, M., Wiese, W., Homann, K.H.: Fullerenes versus soot in benzene flames. Combustion and Flame. **101**, 548–550 (1995)
21. Violi, A., Sarofim, A.F., Truong, T.N.: Mechanistic pathways to explain H/C ratio of soot precursors. Combust. Sci. Technol. **174**, 205–222 (2002)
22. Calcote, H.F.: Mechanisms for the formation of ions in flames. Combustion and Flame. **1**, 385–403 (1957)
23. Fialkov, A.B.: Investigations on ions in flames. Prog. Energy Combust. Sci. **23**, 399–528 (1997)
24. Cody, R.B., Dane, A.J.: Alternative mass reference standards for direct analysis in real time mass spectrometry. Rapid Commun. Mass Spectrom. **30**, 1206–1212 (2016)
25. Cody, R.B.: Follow-up comment on the use of alternative mass reference standards for direct analysis in real time mass spectrometry. Rapid Commun. Mass Spectrom. **30**, 2212–2213 (2016)
26. Lobodin, V.V., Marshall, A.G., Hsu, C.S.: Compositional space boundaries for organic compounds. Anal. Chem. **84**, 3410–3416 (2012)